

Radiation-induced lymphopenia does not impact treatment efficacy in a mouse tumor model



Irma Telarovic^{a,*}; Carmen S.M. Yong^{b,*};
Matthias Guckenberger^b; Jan Unkelbach^b;
Martin Pruschy^{a,*}

^aLaboratory for Applied Radiobiology, Dept. Radiation Oncology, University Hospital Zurich, University of Zurich, Zurich, Switzerland

^bDept. Radiation Oncology, University Hospital Zurich, University of Zurich, Zurich, Switzerland

^cDept. Immunology, University Hospital Zurich, University of Zurich, Zurich, Switzerland

Abstract

Radiation-induced lymphopenia is a common occurrence in radiation oncology and an established negative prognostic factor, however the mechanisms underlying the relationship between lymphopenia and inferior survival remain elusive. The relevance of lymphocyte co-irradiation as critical normal tissue component at risk is an emerging topic of high clinical relevance, even more so in the context of potentially synergistic radiotherapy-immunotherapy combinations.

The impact of the radiotherapy treatment volume on the lymphocytes of healthy and tumor-bearing mice was investigated in a novel mouse model of radiation-induced lymphopenia. Using an image-guided small-animal radiotherapy treatment platform, translationally relevant tumor-oriented volumes of irradiation with an anatomically defined increasing amount of normal tissue were irradiated, with a focus on the circulating blood and lymph nodes. In healthy mice, the influence of irradiation with increasing radiotherapy treatment volumes was quantified on the level of circulating blood cells and in the spleen. A significant decrease in the lymphocytes was observed in response to irradiation, including the minimally irradiated putative tumor area. The extent of lymphopenia correlated with the increasing volumes of irradiation. In tumor-bearing mice, differential radiotherapy treatment volumes did not influence the overall therapeutic response to radiotherapy alone. Intriguingly, an improved treatment efficacy in mice treated with draining-lymph node co-irradiation was observed in combination with an immune checkpoint inhibitor.

Taken together, our study reveals compelling data on the importance of radiotherapy treatment volume in the context of lymphocytes as critical components of normal tissue co-irradiation and highlights emerging challenges at the interface of radiotherapy and immunotherapy.

Neoplasia (2022) 31, 100812

Keywords: Radiotherapy, Normal tissue injury, Lymphopenia, Image-guided small animal radiotherapy platform, Radioimmunotherapy

Introduction

The goal of treatment planning in radiotherapy (RT) is to achieve maximal possible tumor cell killing while sparing the surrounding normal tissue. Due to the high radiosensitivity of lymphocytes, with an *in vitro* LD50 of 2 Gy¹, the immune system is an organ-at-risk with a high susceptibility to RT-induced effects. Radiation-induced lymphopenia (RIL) frequently accompanies RT treatment, with studies reporting its occurrence in 40% to 70% of patients receiving external beam RT². Although the return of the circulating lymphocyte count to the baseline is usually rapid in the post-RT period, numerous recent studies on the clinical level have implicated a negative influence of RIL on the survival outcomes in patients bearing solid tumors³⁻⁵. These findings motivated an interest into developing strategies to minimize the exposure of circulating lymphocytes to ionizing radiation. Such strategies include decreasing the RT treatment volume (RTV), optimizing treatment planning (e.g. sparing the lymphocyte-rich

Abbreviations: ABD, abdomen; CTRL, control; DC, dendritic cells; cDC, conventional dendritic cells; pDC, plasmacytoid dendritic cells; DLN, draining-lymph node; ICI, immune checkpoint inhibitor; mCR, complete response; mPD, progressive disease; mPR, partial response; mRECIST, modified Response Evaluation Criteria in Solid Tumors; mSD, stable disease; NDLN, non-draining lymph node; OS, overall survival; PFS, progression-free survival; RIL, radiation-induced lymphopenia; RT, radiotherapy; RTV, radiotherapy-treatment volume; TBI, total body irradiation; TME, tumor microenvironment; TM, tumor; Treg, regulatory T cell; WBC, white blood cells.

*Corresponding author at: Dept. Radiation Oncology, University Hospital Zurich, Winterthurerstr. 190, CH-8057 Zurich, Switzerland.

E-mail address: martin.pruschy@uzh.ch (M. Pruschy).

Received 3 February 2022; received in revised form 18 May 2022; accepted 23 May 2022

© 2022 Published by Elsevier Inc.
This is an open access article under the CC BY-NC-ND license
(<http://creativecommons.org/licenses/by-nc-nd/4.0/>)
<https://doi.org/10.1016/j.neo.2022.100812>

spleen) and implementing novel RT treatment modalities with a high potential to spare circulating lymphocytes, such as proton therapy and FLASH RT⁶⁻⁹.

The extension of the RT treatment volume into the tumor-draining lymph nodes (DLNs) is standard of care for a number of solid tumors, e.g. head and neck carcinoma¹⁰⁻¹². The rationale for nodal irradiation follows the tendency of many cancers to spread to the DLNs early in the course of the disease. Thus, DLNs frequently harbor clinically evident or occult metastases at the time of diagnosis and may serve as a gateway to metastatic dissemination. At the same time, however, several clinical studies provided inconclusive data on the overall survival benefit of routine nodal irradiation, with a simultaneous increase in RT-related toxicities. These controversial findings call for caution and a potential future evidence-based shift in the standard-of-care based on patient selection, especially in early-stage cancers¹³⁻¹⁸.

The relationship between RT and the immune system is extensively documented on the preclinical and clinical level in the context of radiation poisoning and bone marrow transplantation using total body irradiation (TBI) or large partial-body irradiation¹⁹⁻²¹. More recently, the discovery of immunostimulatory properties of RT facilitated a large number of studies investigating the role of RT as an *in situ* cancer vaccine, with a potential to synergize with novel immunomodulatory agents²²⁻²⁴. Surprisingly, however, there is a complete lack of (pre-)clinical insights investigating clinically relevant tumor-oriented volumes of irradiation with a stepwise increase in the coverage of the surrounding lymph nodes and normal tissue. On the preclinical level, such precise, targeted irradiation of small structures with a high-degree of inter-animal consistency is achievable thanks to the recent development of dedicated image-guided small-animal RT research platforms²⁵. Following computed tomography (CT) imaging, the treatment plan is individually adapted to each animal's specific anatomy, with a clear definition and quantification of target volumes and organs-at-risk. We and others have validated this approach in precision-oriented small animal RT studies, achieving e.g. partial tumor irradiation to model novel methods of fractionation^{26, 27}, targeted heart irradiation with minimal lung co-irradiation to model RT-induced heart toxicity²⁸ and partial lung irradiation to correlate dose-volume parameters with RT-induced lung injury²⁹.

Here, we investigate the impact of translationally relevant, gradually increasing RTVs on the lymphocytes of healthy and tumor-bearing mice, with a focus on organs-at-risk and the relevant lymphoid structures. To our knowledge, this is also the first mouse model to quantify RIL and to probe the impact of RIL and the immune system as part of normal tissue co-irradiation for the tumor response. Our study reveals compelling data on the comparison of RT as a single treatment modality and RT-immunotherapy combination in the context of RIL, thereby highlighting the challenges of designing preclinical models and drawing conclusions at the interface of RT and immunotherapy.

Materials and methods

Cell line and cell culture

MC38 murine colorectal cancer cells were a kind gift from Lubor Borsig (Dept. Physiology, University of Zurich, Switzerland). The cells were cultured in Dulbecco's Modified Eagle Medium (DMEM, Gibco) supplemented with 10% fetal bovine serum (FBS, Gibco) and 1% penicillin/streptomycin (Gibco) at 37°C and 5% CO₂.

Animals

All animal experiments were performed in accordance with Swiss federal and cantonal laws on animal welfare and approved by the Cantonal Veterinary Office Zürich (ZH113/2020). 8-week-old female C57BL/6J mice were

purchased from Envigo. The mice were anesthetized with isoflurane (Attane, Piramal Ltd.) during all interventions (1 L/min oxygen flow rate with 5% isoflurane for induction and 1.5% for maintenance).

Tumor model

MC38 cells in the exponential growth phase (5×10^5) were suspended in a mixture of 120 μ L phosphate-buffered saline (PBS) and 30 μ L Matrigel (Corning) per injection. The cells were injected subcutaneously on the right flank of the mouse (at the midaxillary line just below the ribs). Tumor volumes were estimated from caliper measurements using the formula $V=L*W^2/2$, where V is the volume, L is the length (defined as the largest diameter) and W is the width (defined as the diameter perpendicular to L). RT treatment was initiated once the tumors reached the size of approximately 120 mm³ (8-12 days after injection).

Draining lymph node identification

To map lymphatic drainage of our subcutaneous tumor model, 100 μ L of 1% Evans Blue dye (Sigma-Aldrich) was injected directly into the tumors of untreated mice. After 60 minutes, the mice were killed using CO₂ asphyxiation and the Evans Blue positive lymph nodes were distinguished by eye.

Small animal image-guided radiotherapy research platform

Radiotherapy treatment was performed using the X-RAD SmART (Precision X-Ray Inc.) small animal image-guided radiation research platform. The platform is operated via Pilot software (Precision X-Ray Inc.). Beam characteristics, imaging parameters and the quality assurance procedure are detailed in²⁶. In short, X-RAD SmART is a high-dose delivery platform (treatment performed at 225 kVp and 13 mA with a 0.3 mm Cu filter) with an integrated cone beam CT (CBCT) imaging system. For the 8 \times 12 mm lead collimator used in this study, the system delivers radiation fields with a very sharp penumbra (<1 mm, with the penumbra defined as the distance between 20% and 80% of the maximum dose). The integrated imaging system (40-120 kVp with a 2 mm Al filter) achieves an effective pixel pitch of 0.1 mm at the isocenter, with a typical imaging dose between 1 and 10 cGy. In this study, the "Scout CT" was first used to identify the target and adjust the treatment couch position, followed by a "Soft Tissue Mid Dose" scan preset (40 kVp and 3.0 mA, slice thickness 0.1 mm) to obtain the planning CT. Total dose from imaging thus amounted to 5.9 cGy at the isocenter. All CT images performed in this study were native (non-contrast).

Treatment planning

Treatment planning was performed using a dedicated small animal treatment planning software SmART-ATP (SmART Scientific Solutions B.V.)³⁰. RTV calculations were performed in MIM (MIM Software Inc.). The anesthetized mouse was placed on the treatment couch in the feet-first prone (FFP) to perform the "Scout CT" followed by the planning CT, as described above. Planning CT was then loaded into SmART-ATP, followed by manual tissue segmentation into air, lung, soft tissue and bone to provide the tissue atomic number for dose calculation. In the next step, the treatment plan was designed as described in the "Results" section. Tumor irradiation was performed with two opposing 8 \times 12 mm beams (separated by 180 degrees) with the isocenter placed in the middle of the tumor. Normal tissue irradiation was performed with a single antero-posterior (AP) 8 \times 12 mm beam for each field, with all isocenters set in the tissue-equivalent bed (Superflab, Eckert & Ziegler) on which the mouse was lying during the procedure.

Immune checkpoint inhibition

Anti-mouse α -CTLA4 antibody (clone 9D9, BioXCell) was diluted in PBS to 1 mg/mL and delivered into the intraperitoneal cavity (i.p) in 3×200 μ L doses (1 day prior to RT, day 1 and day 3 after RT). Mouse IgG2b isotype control (clone MPC-11, BioXCell) was delivered using the same dose and schedule.

Hematological analysis

Blood samples were obtained via cardiac puncture with a 7.5% EDTA-coated 26G needle and syringe immediately after CO₂ asphyxiation. 150-300 μ L of the whole blood was transferred to 500 μ L K3 EDTA tubes (Sarstedt). The samples were kept refrigerated and analyzed within 4 hours after sampling.

Hematological analysis was performed in collaboration with the Veterinary Medicine Laboratory (Veterinärmedizinisches Labor, University of Zurich), using the Sysmex XN-1000 Hematology Analyzer (Sysmex).

Immunophenotyping

Tumors, spleens, axillary and inguinal lymph nodes were harvested and processed as follows. Tumors were cut into small pieces with scissors and incubated in 2 mL/sample of extraction buffer [DMEM, 10% FBS, 0.5 mg/mL DNase I (Roche), 1 mg/mL collagenase D (Roche)] for 45 minutes at 37°C. Spleen and lymph nodes were mechanically dissociated and pushed through a 70 μ m cell strainer with a syringe plunger. Red blood cells in the spleen and the blood were then lysed using the ammonium-chloride-potassium (ACK) lysis buffer (Gibco) according to the manufacturer's protocol. To assess cytokine production, single cell suspensions obtained from tumors and lymph nodes were stimulated *ex vivo* for 3.5 hours at 37°C in 200 μ L/sample of activation buffer [DMEM, 10% FBS, 100 ng/mL phorbol 12-myristate 13-acetate (PMA, Sigma-Aldrich), 1 μ g/mL ionomycin (Sigma-Aldrich), 5 μ g/mL brefeldin A (eBioscience)]. Cells were incubated for 30 minutes at 4°C in the extracellular staining mix (see Table S1). Cells were then fixed and permeabilized using the Foxp3/Transcription Factor Staining Buffer Set (eBioscience) according to the manufacturer's instructions, followed by intracellular staining. Samples were acquired on the Cytex Aurora flow cytometer (Cytex) and analyzed using FlowJo software v10.8 (BD Biosciences).

γ H2AX quantification

Blood samples were collected into 500 μ L K3 EDTA tubes (Sarstedt) via cardiac puncture, followed immediately by ACK lysis (Gibco) according to the manufacturer's protocol. Cells were then incubated in the Fc receptor blocking solution (1:100 anti-CD16/32, Invitrogen) for 15 minutes at 4°C, followed by fixation and permeabilization using the Foxp3/Transcription Factor Staining Buffer Set (eBioscience) according to the manufacturer's instructions. Next, the cells were incubated overnight at 4°C with the primary antibody (1:100 anti-phospho-histone H2A.X Ser139 20E3, Cell Signaling). The samples were then incubated with the secondary antibody (1:1000 goat anti-rabbit IgG Alexa Fluor 594, Invitrogen) for 20 minutes at room temperature and acquired on the FACSsymphony flow cytometer (BD Biosciences). The data were analyzed using FlowJo software v10.8 (BD Biosciences).

Statistical analysis

Statistical analysis was performed using Prism v9.3 (GraphPad) and Python v3.7 (Python Software Foundation).

For the efficacy studies, treatments were compared using the Kaplan-Meier survival analysis and the modified Response Evaluation Criteria in Solid Tumors (mRECIST). The endpoint for the Kaplan-Meier survival analysis was defined as the time from treatment start until the tumor volume doubled (for the progression-free survival, PFS) or until the tumor volume reached 6 times the starting volume (for the overall survival, OS). Logrank (Mantel-Cox) test was used to compare the survival curves. The mRECIST methodology was adapted from³¹. For each day d from the start of the treatment until the end of follow up, the tumor volume change $\Delta V_d = 100 * (\frac{V_d - V_{start}}{V_{start}})$ and the average of tumor volume change from day 0 until day d $\Delta \bar{V}_d = \frac{\sum_0^d \Delta V_d}{d}$ were calculated. Best response (BR) was then defined as the minimum value of ΔV_d for $d \geq 7$. Best average response (BAR) was defined as the minimum value of $\Delta \bar{V}_d$ for $d \geq 7$. The criteria for the response were as follows: complete response, mCR: $BR < -95\%$ and $BAR < -40\%$; partial response, mPR: $BR < -50\%$ and $BAR < -20\%$; stable disease, mSD: $BR < 35\%$ and $BAR < 30\%$; progressive disease, mPD: not otherwise categorized.

For the hematological analysis and immunophenotyping, the data are shown as mean \pm standard deviation. Treatment groups are compared using one-way ANOVA test with Dunnett's correction for multiple comparisons. Flow cytometry data is shown either as the percentage of a population, the mean fluorescence intensity (MFI) normalized to the control group or to the expression of the respective marker in the spleen of the same mouse, or the absolute cell count normalized to the control.

All data are collated from at least two independent experiments. For all experiments P value less than 0.05 is considered significant and $P < 0.05$: *, $P < 0.01$: **, $P < 0.001$: ***.

Results

Mouse model of radiation-induced lymphopenia

In contrast to the state of knowledge in response to TBI, only limited data exist on RIL in response to increasing clinically relevant tumor-oriented volumes of irradiation. To achieve a stepwise increase in the degree of RIL, we designed a mouse model of increasing the radiotherapy treatment volume (RTV) in a treatment planning-controlled, strictly defined manner. We considered the DLNs as the organs-at-risk and thus explicitly included or excluded these structures from the treatment plan, as detailed below. As a first step, our model was tested in healthy mice to evaluate the feasibility and robustness of the treatment plan as well as to quantify the influence of increasing RTVs on the circulating blood cells. The treatment groups included sham-irradiated (CTRL), TBI mice and four additional groups irradiated with increasing RTVs (as indicated in Fig. 1A-B and Table 1). All volumes received a dose of 6 Gy with an additional 6 Gy applied to the putative minimal tumor area ("TM"; $RTV = 0.5 \pm 0.2\%$ of the total mouse body volume). Mice also received a minimal radiation exposure of 5.9 cGy by a single CT imaging. Overall, a strong RTV-dependent effect of irradiation was observed on the circulating white blood cells (WBC) as determined by hematological analysis at days 1, 4 and 7 after irradiation (Fig. 1C-G) and on the level of γ H2AX positivity as a biomarker for radiation exposure (Fig. S1A)³². A significant decrease in the WBC count on day 1 after RT was detected in all groups, including the "TM" group, which was surprising, given that a small volume covering only $0.5 \pm 0.2\%$ of the total mouse body volume was irradiated.

In contrast to the larger volumes of irradiation (i.e "TM+ABD+DLN"), the WBC count rapidly returned to the baseline in the "TM" and "TM+DLN" groups by day 4 post irradiation. Within the WBC compartment, lymphocytes and eosinophils underwent the most pronounced decrease in response to RT, with negligible recovery observed at day 7 post irradiation. Monocytes however, showed a more complex response, whereby

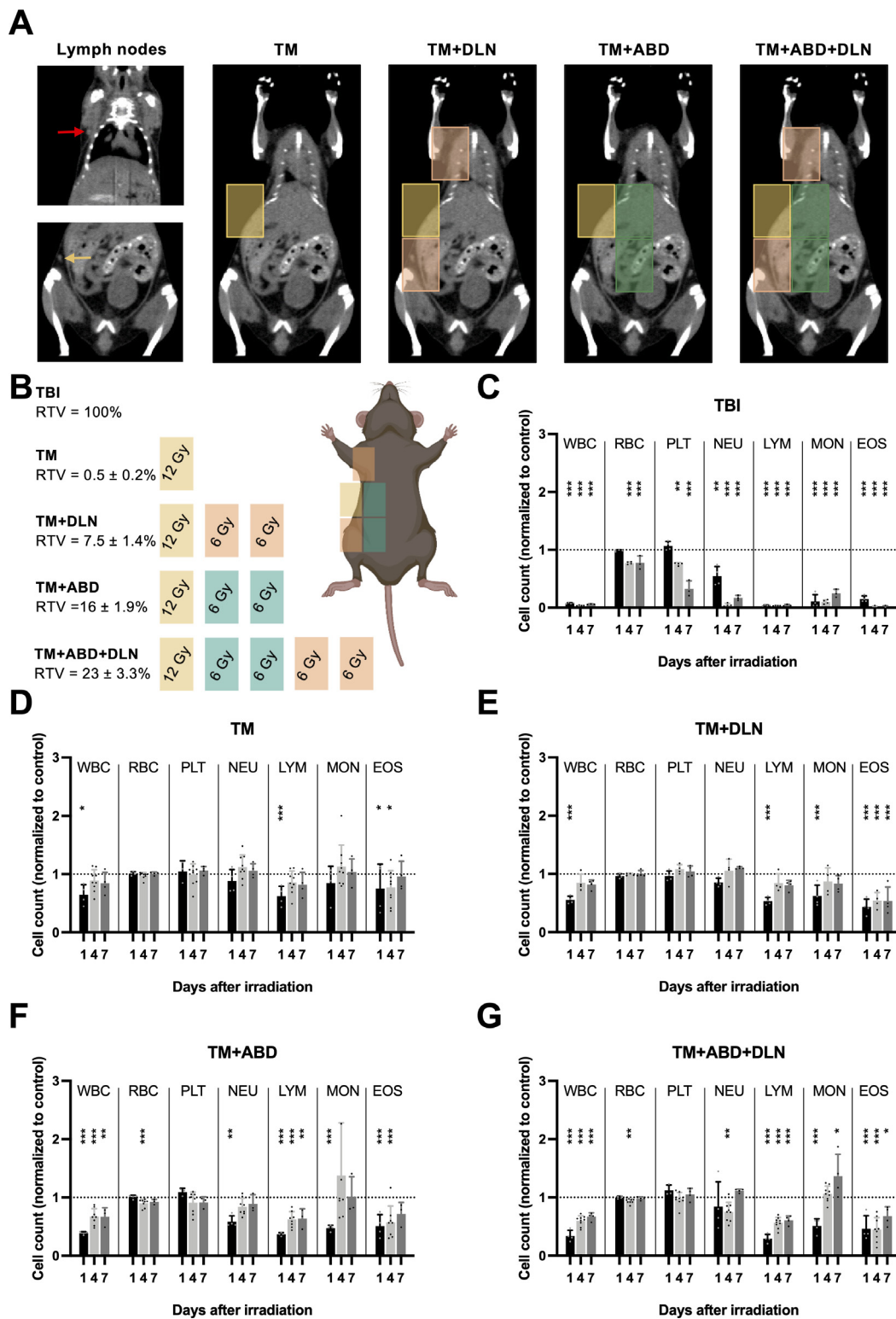


Fig. 1. Mouse model of RIL to evaluate increasing RTVs on circulating blood cells in healthy mice. **A and B**, RT treatment plans in healthy mice designed to induce differential levels of RIL based on an increasing amount of normal tissue co-irradiation (see also Table 1). Yellow rectangle covers the putative tumor area (the “TM” field). Red and yellow arrow point to the axillary and inguinal lymph nodes, respectively, which are targeted with the orange “DLN” fields. Green rectangles cover the extended normal abdominal tissue around the tumor area (“ABD” fields). RTV is defined here as the volume of irradiation/total mouse body volume. **C to G**, Blood cell counts on days 1, 4 and 7 after RT in response to different volumes of irradiation. All counts are normalized to the mean value obtained from 20 sham-irradiated mice (control). The dotted line represents the control, and the significance refers to the comparison with the control. WBC, white blood cells; RBC, red blood cells; PLT, platelets; NEU, neutrophils; LYM, lymphocytes; MON, monocytes; EOS, eosinophils.

Table 1

Description of the treatment plans used for the mouse model of RIL.

Treatment	Description	Dose	RTV (%)
TBI	total body irradiation	6 Gy	100
TM	single-field irradiation modeling a tumor irradiation with minimal extension into the normal tissue	12 Gy	0.5 ± 0.2
TM+DLN	three-field irradiation covering the DLNs (inguinal and proper axillary lymph nodes, clearly distinguishable in CT imaging as seen in Fig. 1A), modeling nodal irradiation	12 Gy to TM 6 Gy to DLN	7.5 ± 1.4
TM+ABD	three-field irradiation covering a part of the healthy abdominal area, modeling a conservative tumor irradiation with extensive coverage of the surrounding normal tissue	12 Gy to TM 6 Gy to ABD	16 ± 1.9
TM+ABD+DLN	five-field irradiation covering a part of the healthy abdominal area and the DLNs, modeling a conservative tumor irradiation with nodal irradiation	12 Gy to TM 6 Gy to ABD 6 Gy to DLN	23 ± 3.3
CTRL	control group, sham-irradiation (including CT imaging)	-	-

RTV is defined as the volume of irradiation/total mouse body volume.

reduced cell counts at day 1 post irradiation were overly compensated at later timepoints, with numbers reaching above baseline in both the “TM+ABD” and “TM+ABD+DLN” groups (Fig. 1F-G). Red blood cells and platelets demonstrated very little sensitivity to irradiation, with a significant decrease only observable at day 4 and day 7 in the “TBI” group, unsurprisingly given that irradiation also sterilizes the bone marrow. Thus, a functioning mouse model of RIL could be established demonstrating RTV-dependent dynamics of circulating blood cell counts.

Large volume of irradiation induces prolonged lymphopenia in healthy mice

Given the complexity of the immune system and having only performed a broad analysis of the circulating immune compartment, we characterized RIL in response to irradiation with the smallest and the largest RTVs (“TM” vs “TM+ABD+DLN”, Fig. 2A) in more detail. We therefore performed detailed immunophenotyping of the blood and the spleen at various timepoints until day 21 after RT (Fig. 2 and Fig. S1). In the “TM” group, a significant decrease in the number of circulating lymphocytes (Fig. 2B) and eosinophils (Fig. S1B) on day 1 after irradiation was identified, followed by a rapid return to the baseline at day 4 for lymphocytes (Fig. 2B) and day 7 for eosinophils (Fig. S1B). In the “TM+ABD+DLN” group, we observed a stronger decrease early after RT in circulating lymphocytes in comparison to the “TM” group, however this effect was restricted to the periphery, as cell numbers remained unchanged in the spleen throughout all timepoints (Fig. 2B-C). Interestingly though, while neutrophil and monocyte subpopulations gradually returned to the basal range within this time frame, lymphocyte and eosinophil subpopulations were unable to completely recover during the follow-up time of 21 days after irradiation (Fig. 2B and Fig. S1B). In a more detailed analysis of lymphocyte subpopulations in the blood, stable percentages of CD4⁺ and CD8⁺ cells within the T cell compartment were observed at days 4 and 9 after irradiation (Fig. 2C). At the later timepoint, the percentage of CD4⁺ T cells and more specifically, CD4⁺FOXP3⁺ regulatory T cells (Tregs) significantly decreased in the “TM” group, which resulted in a significant increase in the CD8⁺/CD4⁺ ratio. Overall, these results demonstrate RTV- and cell type-dependent reduction and repopulation of the circulating immune cell compartment in response to irradiation, resulting in a shift in the ratio of anti-tumoral CD8⁺ T cells to immunosuppressive Tregs.

Tumor response to radiotherapy is not affected by the degree of radiation-induced lymphopenia

To investigate the impact of increasing RTVs and subsequently differential circulating immune cell compartments on the tumor response, MC38 murine colon carcinoma cells were implanted on the right flank of mice at the midaxillary line just below the ribs and irradiated once reaching a tumor volume of 120 mm³. The proper axillary and the inguinal lymph node as the DLNs were validated by injecting the Evans Blue dye into the tumor (Fig. 3A) and mice were irradiated with three increasing RTVs, as described in the previous section (Fig. 1A, 3B, “TM”, “TM+DLN” and “TM+ABD+DLN”). A significant tumor growth delay was induced by all three RTVs in comparison to sham-irradiated tumors (Fig. 3C). In order to control for the same volume of irradiation but to avoid irradiation of the DLNs, we included targeting of non-draining lymph nodes (NDLNs) instead of the DLNs (Fig. 3B, “TM+NDLN” and “TM+ABD+NDLN”). Surprisingly, no significant differences in tumor growth between the five treatment groups were observed, as demonstrated by comparison of progression-free survival (PFS) and overall survival (OS) in response to irradiation with the different RTVs (Fig. 3C and Fig. S2). Likewise, mRECIST analysis did not indicate a differential treatment response (Fig. 3D-E). Thus, the differential RTVs did not affect the overall therapeutic response to irradiation.

A restricted radiotherapy treatment volume correlates with a shift towards an immunostimulatory tumor microenvironment

The current interest in combining RT with immunotherapy asks for a detailed analysis of RT- dependent changes that might predispose the tumor microenvironment (TME) towards successful immunotherapeutic intervention. To investigate immunophenotypic changes in the tumor as well as secondary lymphoid organs, immune cell analysis was performed for the treatment groups “TM”, “TM+ABD+DLN” and “TM+ABD+NDLN” of tumor-bearing mice at day 4 after irradiation (Fig. 4A). The changes in the blood cell count in response to irradiation with increasing RTVs in the tumor-bearing mice followed a similar pattern as in healthy mice (Fig. 4B and Fig. 1D, G respectively). Interestingly and despite the lack of a differential tumor growth response in dependence of the RTV (see above), we observed a significant decrease in the number of T lymphocytes in the tumors following irradiation with a large RTV (“TM+ABD+DLN” and “TM+ABD+NDLN”) in comparison to the number of T lymphocytes

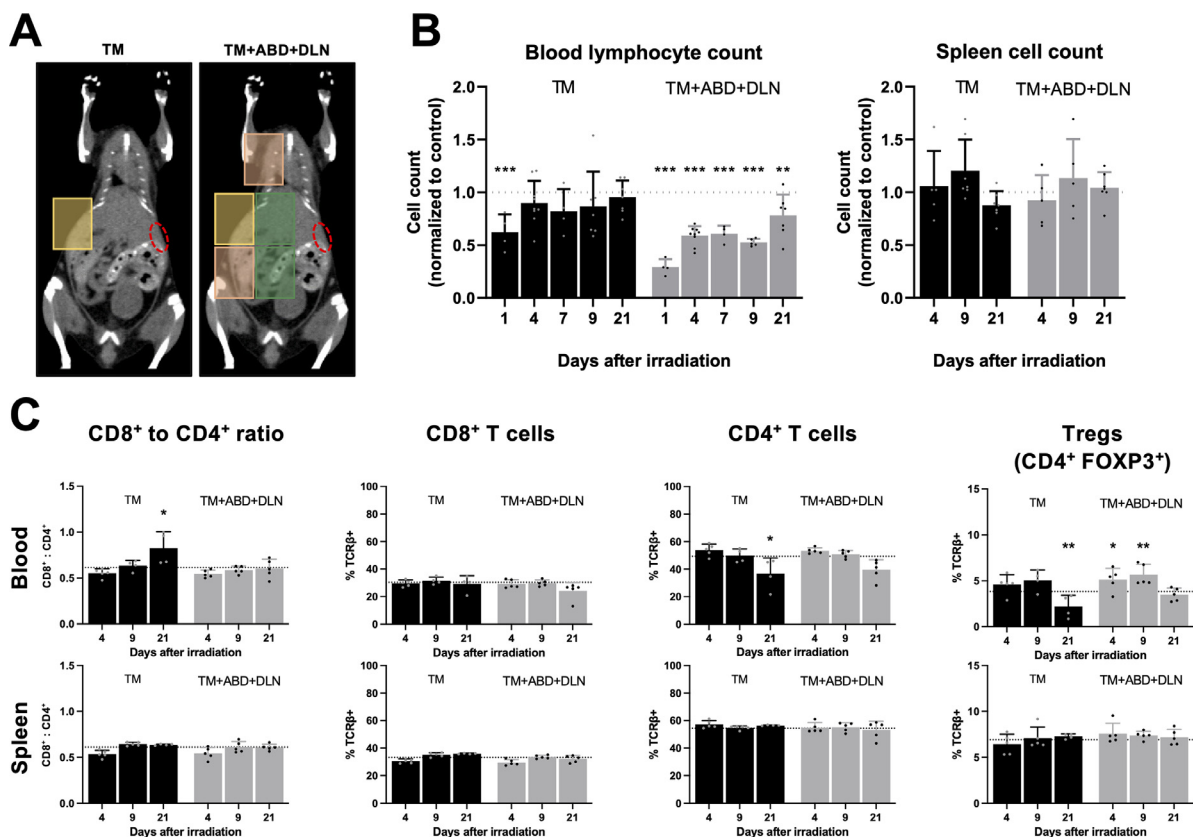


Fig. 2. Irradiation with large RTVs induces prolonged lymphopenia. Extended cell analysis over 21 days after irradiation was performed in healthy mice treated with the “TM” and “TM+ABD+DLN” RTVs. **A**, Treatment plans with the spleen contoured in red. **B**, Blood lymphocyte count and spleen cell count. **C**, Analysis of lymphocyte subsets in the blood and the spleen. All absolute counts are normalized to the mean value obtained from 9 sham-irradiated mice (control). The dotted line represents the control, and the significance refers to the comparison with the control.

following small volume irradiation (“TM” group) (Fig. 4C, first row). Furthermore, an increase in the relative amount of CD8⁺ T cells and a corresponding decrease in the relative amount of CD4⁺ T cells in the tumor was identified in the tumors of mice treated with the small RTV, resulting in an increased CD8⁺ to CD4⁺ ratio in the tumors of these mice. Interestingly, no differences in the relative abundance of Tregs were observed following irradiation with the different RTVs. Similar to the RTV-dependent drop of T lymphocytes in the tumor, a trend towards a volume-dependent decrease in the number of T lymphocytes in both the DLNs and NDLNs, as well as in the blood was identified in response to irradiation with the extended RTVs in comparison to mice treated with the small, tumor-directed RTV (Fig. 4C, rows 2-4).

Tumor response to radioimmunotherapy is affected by draining lymph node irradiation and not by the radiotherapy treatment volume

Based on the improved (anti-tumorigenic) immune phenotype in the tumors treated with the small tumor-directed volume of irradiation, but lack of an improved tumor growth response, we next investigated how differential RTVs might affect the tumor response when combining RT with immunotherapy. Tumor-bearing mice were treated with three doses of α -CTLA4, an immune checkpoint inhibitor (ICI), which previously demonstrated a well-established synergism with radiotherapy in the MC38 tumor model³³. The tumor response was probed as part of a combined radiotherapy treatment modality with the “TM”, “TM+ABD+DLN” and “TM+ABD+NDLN” treatment plans (Fig. 5A). No differential tumor response could be detected between the groups of mice treated with the small

RTV “TM” and the large RTV “TM+ABD+NDLN” when combined with the ICI. Interestingly though, the tumor response was strongly improved on combined treatment with the RTV “TM+ABD+DLN” in comparison to the RTVs “TM” and “TM+ABD+NDLN”. Median PFS (time to reach $2 \times V_{\text{start}}$) was not reached within 30 days after irradiation in the group of mice treated with ICI and the RTV “TM+ABD+DLN”, as opposed to the mice treated with ICI and the RTVs “TM” and “TM+ABD+NDLN” (median PFS 14.5 and 18 days, respectively) (Fig. 5B, D). This strongly improved treatment response in the “TM+ABD+DLN+ICI” was further supported by the mRECIST analysis, which classified 8 out of 9 mice in the “TM+ABD+DLN+ICI” group as responders, with 4 mCRs, 1 mPR and 3 mSDs (Fig. 5C, D). In contrast, no mCRs or mPRs could be identified in the “TM+ICI” group, with only 3 mice classified as mSD and the remaining 6 as mPD. Unlike the “TM+ABD+DLN+ICI” group, only 1 mCR, 2 mPRs, 2 mSDs and 4 mPDs could be identified in the “TM+ABD+NDLN+ICI” group, indicating a differential response between irradiation of the DLN and NDLN in combination with ICI in this tumor model.

To identify putative differences in the immunophenotype that may have predisposed the TME to an enhanced response to α -CTLA4 treatment, extended immunophenotypic analysis of the DLNs, NDLNs and tumors was performed at day 4 after irradiation with the different RTVs. Intriguingly, we observed a significant increase in the proliferation status of CD8⁺ T cells (as denoted by the expression of Ki67) exclusively in the lymph nodes of mice treated with the “TM+ABD+DLN” RTV (Fig. 5E). Of note, irradiation with the “TM+ABD+DLN” RTV increased expression of the proliferation marker Ki67 not only in the irradiated DLNs, but also in the non-irradiated NDLNs. On the other hand, irradiation with the “TM+ABD+NDLN”

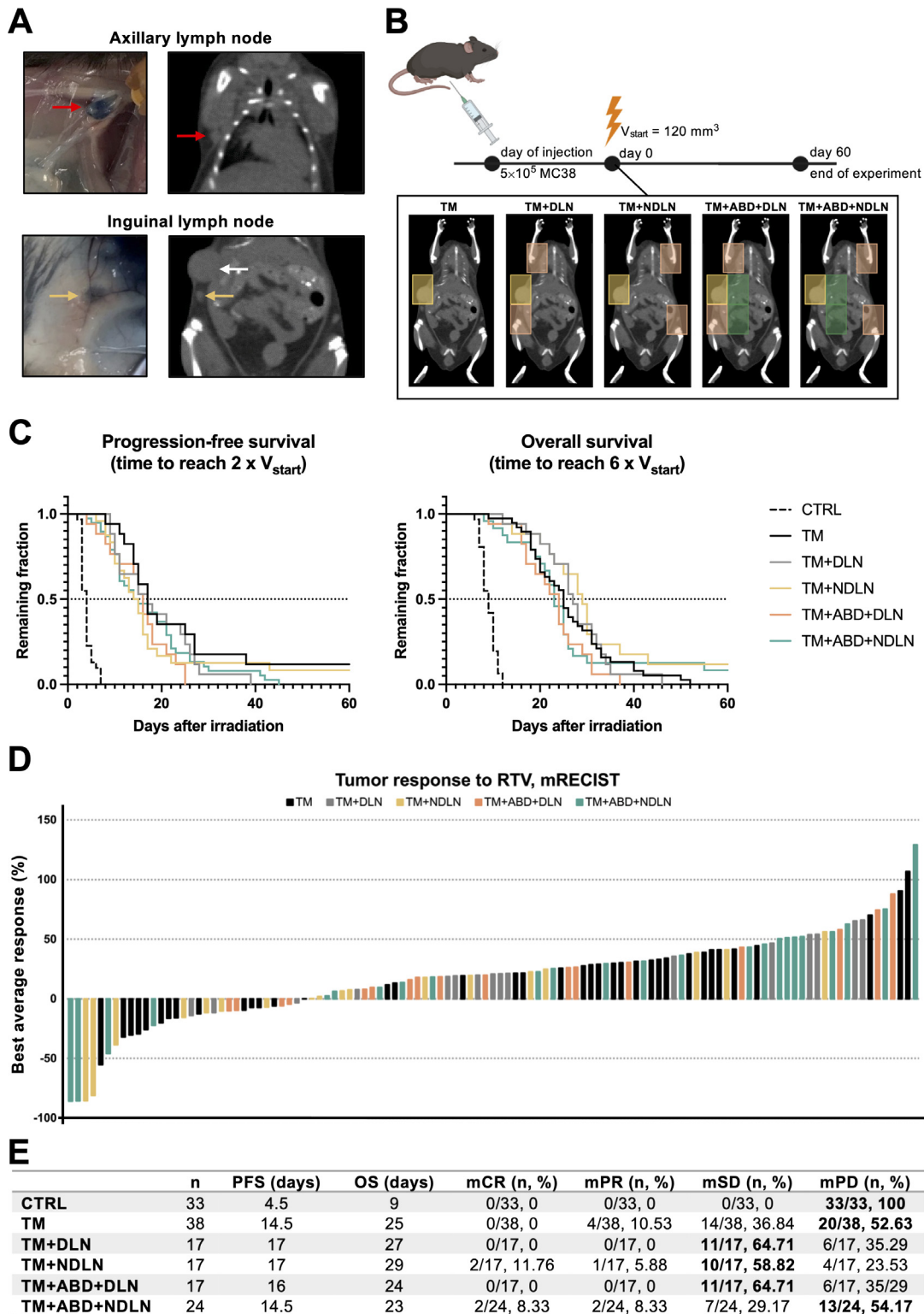


Fig. 3. Tumor response to radiotherapy is not affected by the degree of radiation-induced lymphopenia. **A**, Evans Blue dye was used to confirm the axillary (red arrow) and inguinal (yellow arrow) lymph nodes as the DLNs in the subcutaneous tumor-bearing mice (white arrow points at the tumor). **B**, Design of experiment: RT treatment was initiated once the tumors reached the size of 120 mm^3 and tumor growth was followed over a period of 60 days post treatment start. Five different RTVs were compared, as described in the Results section. **C**, Tumor response to the treatment represented with Kaplan-Meier survival curves. PFS is defined as the time to reach $2 \times V_{start}$; OS is defined as the time to reach $6 \times V_{start}$. **D**, mRECIST analysis visualized in a waterfall plot. Each bar represents a single mouse, with the height corresponding to the “Best average response” value obtained as described in the Materials & Methods section. **E**, Quantitative values derived from the Kaplan-Meier and mRECIST analyses. For each RTV, the highest number of mice/RTV classified to the same mRECIST category is in bold.

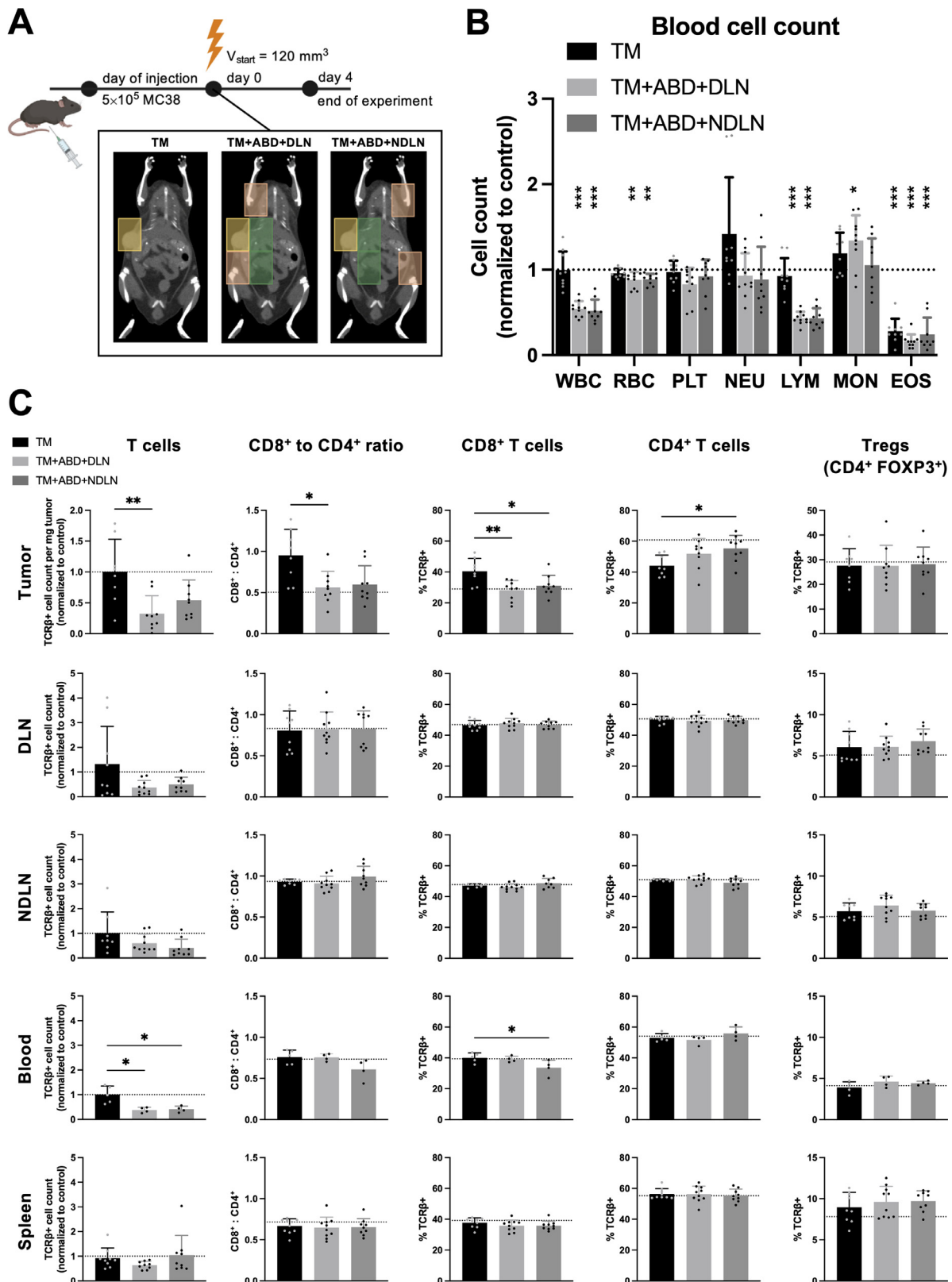


Fig. 4. The analysis of the immune phenotype changes in the tumor, lymphoid organs and the blood in response to different volumes of irradiation. **A**, Design of experiment: RT treatment was initiated once the tumors reached the size of 120 mm³ and the organs were harvested on day 4 after RT. **B**, Hematological analysis. **C**, Comparison of the absolute lymphocytes counts and the lymphocyte compartment composition in the tumor, lymph nodes, blood and the spleen. All absolute counts are normalized to the mean value obtained from 8 sham-irradiated mice (control). The dotted line represents the control, and the significance refers to the comparison with the control in B, and to the comparison in between the groups in C.

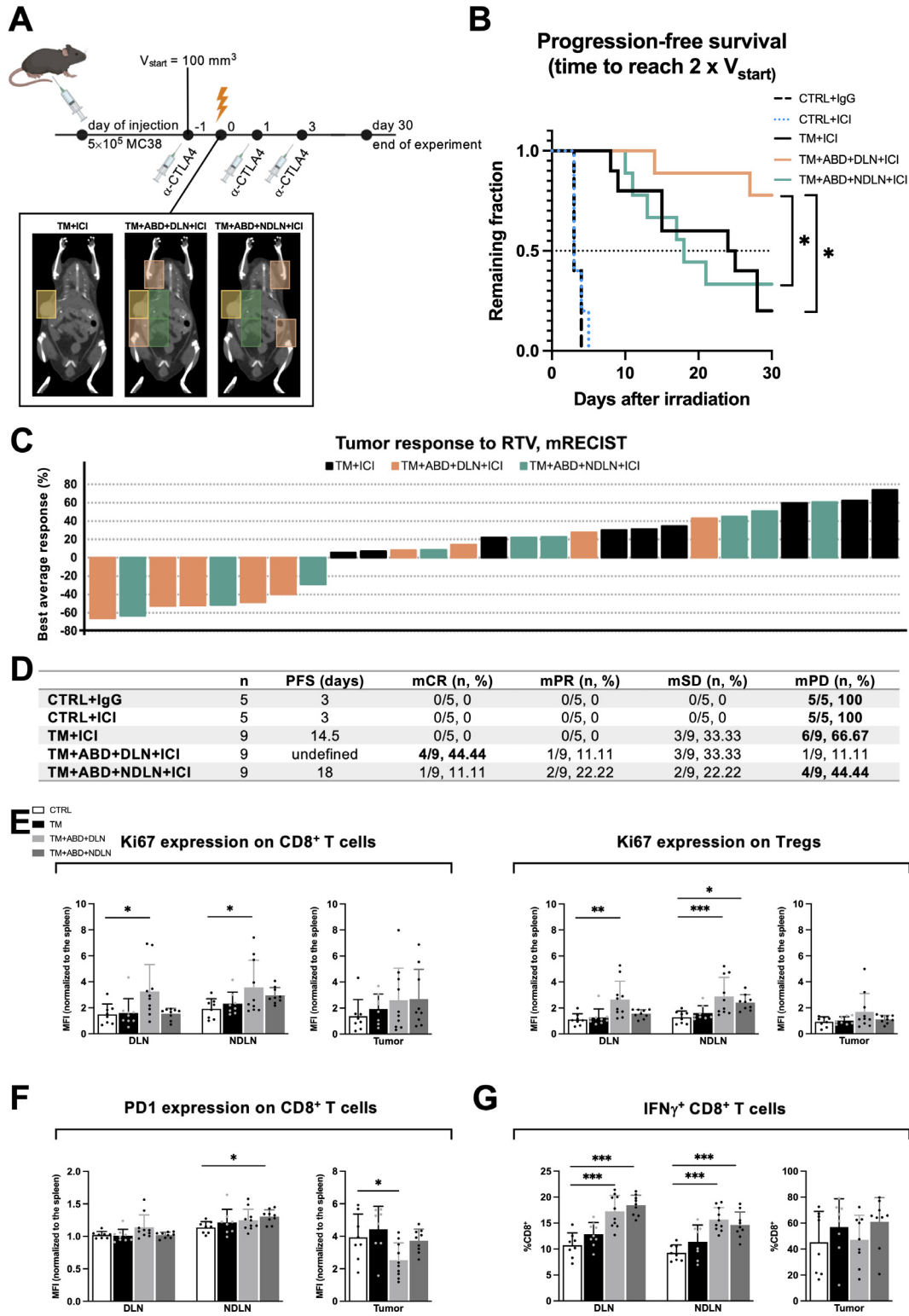


Fig. 5. Tumor response to radiotherapy in the presence of immune checkpoint inhibition is affected by the draining lymph node irradiation, and not by the radiotherapy treatment volume. **A**, Design of experiment: α -CTLA4 treatment was initiated once the tumors reached the size of 100 mm³ (day -1). RT treatment occurred 24 hrs thereafter (day 0). Tumor growth was followed over a period of 30 days after irradiation **B**, Tumor response to treatment represented with the Kaplan-Meier survival curve, with the PFS defined as the time to reach $2 \times V_{start}$. **C**, mRECIST analysis visualized in a waterfall plot. Each bar represents a single mouse, with the height corresponding to the “Best average response” value obtained as described in the Materials & Methods section. **D**, Quantitative values derived from the Kaplan-Meier and mRECIST analyses. For each RTV, the highest number of mice/RTV classified to the same mRECIST category is in bold. **E**, Analysis of lymphocytes in ICI-naïve mice. Treatment groups are compared to the control. MFI values are normalized to the expression of the respective marker in the spleen of the same mouse.

RTV did not induce a significant increase in Ki67 expression in either lymph nodes. A similar pattern was observed in regulatory T cells, whereby Ki67 expression was significantly increased on treatment with the RTV “TM+ABD+DLN” in both DLNs and NDLNs. An increase in the RTV “TM+ABD+NDLN” group was only detected in the irradiated NDLNs. Surprisingly, enhanced Ki67 expression was only observed in the LNs, as we did not observe significant differences in the proliferation status of tumor-infiltrating T cells (Fig. 5E).

The expression of the exhaustion marker PD1 on CD8⁺ T cells residing in the DLN and NDLNs did not significantly differ between the different treatment groups, apart from a slight increase in the NDLNs of the mice treated with the RTV “TM+ABD+NDLN” (Fig. 5F). Interestingly though, a significant decrease in the expression of PD1 was detected on CD8⁺ T cells present in the tumors treated with the RTV “TM+ABD+DLN”, which was not observed in the “TM+ABD+NDLN” group.

Furthermore, the ability of T lymphocytes to produce the pro-inflammatory cytokine IFN γ was determined to probe whether the phenotypic changes induced by the differing RTVs had any functional consequences. The production of IFN γ by CD8⁺ T cells was increased in both the DLNs and NDLNs of mice in response to irradiation with both extended RTVs but not in sham-irradiated mice and mice irradiated with “TM” RTV (Fig. 5G). No differences in IFN γ production in the tumors were identified at this time point.

Eventually, detailed analysis of the dendritic cell (DC) composition uncovered an increase of conventional DCs (cDCs) in the LNs of mice treated with the “TM” RTV and a trend towards a decrease in cDCs in the LNs of the mice treated with the “TM+ABD+DLN” RTV (Fig. S5A). Specifically, the cross-presenting cDC1 subpopulation was significantly reduced only in the DLNs of the mice treated with the “TM+ABD+DLN” RTV. Even though the “TM+ABD+DLN” RTV resulted in a quantitative decrease of cDC1, in depth characterization of these cells demonstrated an upregulation of markers associated with antigen processing and presentation.

Discussion

Lymphopenia and treatment-induced reduction of lymphocytes as an immunological side effect of radiotherapy are emerging negative prognostic factors for multiple solid tumor entities³⁻⁵. Although immunosuppression and the resulting susceptibility to infections are certainly major contributors, recent insights on lymphocytes as the key players in anti-tumor immunity offer novel explanations for the link between RIL and inferior treatment outcome. Thereby, RIL might serve not only as a prognostic, but also as a predictive biomarker for radioimmunotherapy combinations³⁴. In this context, circulating blood, highly vascularized tissues and lymphoid structures as the lymphocyte-related organs at risk (LOARs, as described in³⁵) are in focus. Despite the clinical interest to elucidate the relevance of the interaction between the RTV and the immune system, preclinical research is lacking. Here we present a novel mouse model to study the effects of differential RTVs on the lymphocytes of healthy and tumor-bearing mice.

In contrast to previous studies by others investigating partial and total body irradiation^{19, 20}, we used a small animal RT platform with CT-image-guidance to plan RTVs and to precisely irradiate the tumor and an increasing volume of the surrounding normal tissue in our mouse model, thereby mimicking clinical treatment planning. The gradual increase of normal tissue co-irradiation allowed for a detailed analysis and direct comparison of the effects of different levels of lymphopenia. Each treatment plan was adapted to the individual anatomy of each animal, thus ensuring the consistency in the volume of irradiation and the inclusion or exclusion of lymphocyte-rich organs, including the lymph nodes.

Surprisingly, already the smallest RTV, whereby only 0.5% of the total mouse body is irradiated, induced significant lymphopenia in healthy mice

at the early timepoint, thereby illustrating the potential magnitude of RTV-induced effects. This unexpected response might be due to the relatively long treatment time with a dose rate of 3 Gy/min (approximately 4 minutes for the “TM” field) compared to the blood turnover rate of 4.5 seconds in mice, suggesting that a large pool of blood lymphocytes might indeed receive a lethal dose during such a treatment³⁶. A significant increase in the level of γ H2AX expression already in the “TM” RTV supports this hypothesis. On the other hand, the persistence of lymphopenia over the 21 days of follow up in the blood of the mice treated with large RTV is difficult to understand and might be linked to the complex recirculation kinetics of lymphocytes, which largely remain elusive³⁶. Notably, prolonged lymphopenia (persisting over a year after external beam RT) is also observed in human patients, with an impairment in the IL-7 and IL-15 compensatory response proposed as the likely cause, although the exact mechanism remains unknown³⁷.

In vivo radiosensitivity of different lymphocyte subsets is an ongoing topic of investigation, with Tregs emerging as the more radioresistant subset, although data are not conclusive and conflicting observations have been reported^{35, 38-40}. In the immunophenotyping of the lymphocyte compartment of healthy mice in this study, we did not observe any changes indicative of differential radiosensitivity between the T cell subsets. A modest decrease in the Treg subset of CD4⁺ T cells was only observed at a later timepoint. However, it is unlikely that such an effect can be attributed to a difference in the intrinsic radiosensitivity of Tregs, as many other factors, such as proliferation, repopulation, redistribution from different compartments and even changes in the expression of the Treg-defining marker FOXP3 could contribute to the circulating cell count in this time frame³⁹. Importantly, unlike in our model, the majority of previous studies were based on *ex vivo* blood irradiation or TBI, and not on smaller, tumor-oriented volumes of irradiation. The distribution of specific immune subsets differs in different peripheral organs, which is based on their function and maturation state. Thus, RTVs that selectively target the niches specific for an immune subset, may contribute to the phenotypic changes we observed. Eventually, location of the tumor relative to such niches will have to be taken into consideration on the individual level.

The response of the other circulating blood cells to the increasing RTVs mostly corresponded to existing data derived from mice treated with TBI⁴¹. Unexpectedly, however, eosinophils in our model responded to an increasing RTV similarly to lymphocytes, with a significant and sustained decrease, thus demonstrating high susceptibility to radiation-induced effects consistently over the follow up time of 21 days. Taking the emerging role of eosinophils in the RT-induced anti-tumor immunity into consideration⁴², this previously unreported finding warrants further investigation.

Surprisingly, no impact of increasing RTVs and concomitant RIL was observed on the tumor response to RT as a single treatment. By controlling for the level of RIL with irradiation of the NDLN, we could also identify lack of a contribution of DLN-irradiation on the tumor response using RT as single treatment modality. Buchwald *et al.* similarly observed no impact of DLN irradiation on the local control but on abscopal responses, in their highly immunogenic bacterial glycoprotein-expressing B16F10GP model⁴³. These results however contrast the findings of Marciscano *et al.*⁴⁴, who reported a decrease in the median survival of mice treated with DLN irradiation in their highly immunogenic MC38-OVA model (see also below). The discrepancy most probably stems from the differences in radiosensitivity and immunogenicity between the different cell lines, with highly specific anti-tumor immunity in the OVA-antigen-oriented animal systems. In the analysis of the intratumoral immune cell composition, however, both we and others detected favorable changes in the immune phenotype in response to tumor-only irradiation compared to the DLN irradiation.

To exploit the shift towards a presumably more immunostimulative environment (with the “TM”-only RTV), RT was combined with an ICI. To our surprise, irradiation with the “TM+ABD+DLN” RTV in combination

with α -CTLA4 induced a drastic improvement in the tumor control in comparison to the combined treatment modality with the small “TM” or the large “TM+ABD+NDLN” RTVs. This result was unexpected, given that DLNs are known to be lymphoid structures in which T cell priming occurs⁴⁵. The mechanisms underlying this synergistic effect are still under investigation. Irradiation of the DLN might generate both physical space as well as increased availability of necessary cytokines required for proliferation, such as IL-7⁴⁶, thereby supporting an increased proliferation of both CD8⁺T cells and Tregs in the lymph nodes of mice irradiated with the RTV “TM+ABD+NDLN”. In the absence of ICI, the tumor response to DLN irradiation was similar to that of “TM” alone. Given that one major function of α -CTLA4 is its ability to deplete Tregs *in vivo*⁴⁷, the addition of ICI in the “TM+ABD+NDLN” might deplete Tregs within the DLN, freeing up cytokines and thus promoting a greater expansion of proliferating, antitumorigenic CD8⁺T cells. Irradiation of the NDNLN with the RTV “TM+ABD+NDLN” in combination with the ICI, did not result in an improved tumor response in comparison to irradiation with the RTV “TM”+ICI. Thus, the proliferating CD8⁺T cell population in the DLN irradiated as part of the RTV “TM+ABD+NDLN” may be a result of clonally expanding antigen-primed T cells, which are essential in mounting the antitumor response. Furthermore, CTLA4 interferes with binding of the T-cell co-stimulatory molecule CD28 to its ligands CD80/86 on the DCs. Thus, the potential stimulatory effect of irradiation on the maturation of cDC1s might only become relevant in the context of combined radioimmunotherapy. While this data suggests that RIL in specific secondary lymphoid organs in addition to ICI may be worth investigating, care must be taken as different mechanisms between murine and human ICIs may prevent direct translation into patients^{48, 49}.

A strong negative impact of DLN-co-irradiation on the combined treatment modality with α -CTLA4 was previously demonstrated by Marciscano et al⁴⁴. However, in our own study and in contrast to the former investigations, DLNs were irradiated with only a reduced (50%) dose relative to the total dose applied to the tumor, which is often also the case in the clinical setting of elective lymph node irradiation. Thereby, we assume that the DLNs were not completely sterilized. These discrepancies illustrate the complexity of combining a systemic treatment modality with stereotactic RT, that is locally applied and has to take the individual tumor entity and its localization into consideration. Likewise, dose and fractionation schedule of RT, the type of ICI and timing of ICI relative to RT will have to be investigated in further mechanistic detail in order to translate our findings towards the clinics. Despite the limitations, this work contributes to better understanding the complexity underlying the interface of RT and the immune system.

Conclusion

Here we successfully developed and characterized in detail a novel mouse model of RIL, whereby we compared different volumes of irradiation with the immune system as an organ-at-risk in focus. Moreover, we report intriguing and hypothesis-generating findings in tumor-bearing mice, which together with the previous studies indicate that the impact of RIL and DLN irradiation on the treatment response might greatly depend on the context. Thus, our study serves to further motivate detailed follow up (pre)clinical investigations to fully comprehend the compelling topic of the immune system as an organ-at-risk in RT.

Declaration of interests

The authors declare that they have no known competing financial interests or personal relationships that could have appeared to influence the work reported in this paper.

CRedit authorship contribution statement

Irma Telarovic: Conceptualization, Formal analysis, Investigation, Writing – review & editing, Resources, Funding acquisition. **Carmen S.M. Yong:** Formal analysis, Investigation, Writing – review & editing. **Matthias Guckenberger:** Resources. **Jan Unkelbach:** Methodology. **Martin Pruschy:** Conceptualization, Writing – review & editing, Supervision, Resources, Funding acquisition.

Acknowledgements

We thank Onur Boyman for helpful discussions and technical support. This work was supported by the MD-PhD scholarship of the [Swiss Academy of Medical Sciences \(MD-PhD-4820-06-2019\)](#) sponsored by the Swiss Cancer Research Foundation (to I.T.), and by the grants from the [Swiss Cancer Research Foundation \(KFS-5301\)](#) and the [Swiss National Science Foundation \(310030_189285\)](#) (to M.P.). Figures were created using BioRender.com (publication license KA23HUAZGI).

Supplementary materials

Supplementary material associated with this article can be found, in the online version, at doi:[10.1016/j.neo.2022.100812](https://doi.org/10.1016/j.neo.2022.100812).

References

- Nakamura N, Kusunoki Y, Akiyama M. Radiosensitivity of CD4 or CD8 positive human T-lymphocytes by an in vitro colony formation assay. *Radiat Res* 1990;**123**(2):224–7.
- Ellsworth SG. Field size effects on the risk and severity of treatment-induced lymphopenia in patients undergoing radiation therapy for solid tumors. *Adv Radiat Oncol* 2018;**3**(4):512–19.
- Dai D, Tian Q, Shui Y, Li J, Wei Q. The impact of radiation induced lymphopenia in the prognosis of head and neck cancer: A systematic review and meta-analysis. *Radiother Oncol* 2022.
- Damen PJ, Kroese TE, van Hillegersberg R, Schuit E, Peters M, Verhoeff JJ, et al. The influence of severe radiation-induced lymphopenia on overall survival in solid tumors: a systematic review and meta-analysis. *Int J Radiat Oncol Biol Phys* 2021;**111**(4):936–48.
- Upadhyay R, Venkatesulu BP, Giridhar P, Kim B, Sharma A, Elghazawy H, et al. Risk and impact of radiation related lymphopenia in lung cancer: A systematic review and meta-analysis. *Radiother Oncol* 2021;**157**:225–33.
- Shiraishi Y, Fang P, Xu C, Song J, Krishnan S, Koay EJ, et al. Severe lymphopenia during neoadjuvant chemoradiation for esophageal cancer: A propensity matched analysis of the relative risk of proton versus photon-based radiation therapy. *Radiother Oncol* 2018;**128**(1):154–60.
- Routman DM, Garant A, Lester SC, Day CN, Harmsen WS, Sanheuzza CT, et al. A comparison of grade 4 lymphopenia with proton versus photon radiation therapy for esophageal cancer. *Adv Radiat Oncol* 2019;**4**(1):63–9.
- Alexandru M, Rodica A, Dragos-Eugen G, Mihai-Teodor G. Assessing the spleen as an organ at risk in radiation therapy and its relationship with radiation-induced lymphopenia: A retrospective study and literature review. *Adv Radiat Oncol* 2021;**6**(6):100761.
- Jin J-Y, Gu A, Wang W, Oleinick NL, Machtay M. Ultra-high dose rate effect on circulating immune cells: A potential mechanism for FLASH effect? *Radiother Oncol* 2020;**149**:55–62.
- Biau J, Lapeyre M, Troussier I, Budach W, Giralt J, Grau C, et al. Selection of lymph node target volumes for definitive head and neck radiation therapy: a 2019 update. *Radiother Oncol* 2019;**134**:1–9.
- Loganadane G, Truong PT, Taghian AG, Tešanović D, Jiang M, Geara F, et al. Comparison of nodal target volume definition in breast cancer radiation therapy according to RTOG versus ESTRO atlases: a practical review from the TransAtlantic Radiation Oncology Network (TRONE). *Int J Radiat Oncol Biol Phys* 2020;**107**(3):437–48.

12. Hall WA, Paulson E, Davis BJ, Spratt DE, Morgan TM, Dearnaley D, et al. NRG oncology updated international consensus atlas on pelvic lymph node volumes for intact and postoperative prostate cancer. *Int J Radiat Oncol Biol Phys* 2021;**109**(1):174–85.
13. Dodwell D, Taylor C, McGale P, Coles C, Duane F, Gray R, et al. Abstract GS4-02: Regional Lymph Node Irradiation in Early Stage Breast Cancer: An EBCTCG Meta-Analysis of 13,000 Women in 14 Trials. San Antonio Breast Cancer Symposium: AACR; 2019. p. GS4–G02.
14. Koontz BF, Dal Pra A. Shifting the curtain—can we make sense of the whole pelvis controversy? *Int J Radiat Oncol Biol Phys* 2020;**106**(3):534–6.
15. Ladbury C, Goodman KA, Scheffer TE, Olsen JR. Anal cancer in the era of dose painted intensity modulated radiation therapy: Implications for regional nodal therapy. *Seminars in Radiation Oncology*. Elsevier; 2019.
16. Poortmans PM, Weltens C, Fortpied C, Kirkove C, Peignaux-Casasnovas K, Budach V, et al. Internal mammary and medial supraclavicular lymph node chain irradiation in stage I–III breast cancer (EORTC 22922/10925): 15-year results of a randomised, phase 3 trial. *Lancet Oncol* 2020;**21**(12):1602–10.
17. Senkus E, Cardoso MJ, Kaidar-Person O, Łacko A, Meattini I, Poortmans P. De-escalation of axillary irradiation for early breast cancer—Has the time come? *Cancer Treat Rev* 2021;**101**:102297.
18. Weiner AB, Ko OS, Zhu A, Spratt DE, Hu JC, Schaeffer EM. National practice patterns for lymph node irradiation in 197,000 men receiving external beam radiotherapy for localized prostate cancer. *Urologic Oncology: Seminars and Original Investigations*. Elsevier; 2019.
19. Ossetrova NI, Condliffe DP, Ney PH, Krasnopolsky K, Hieber KP, Rahman A, et al. Early-response biomarkers for assessment of radiation exposure in a mouse total-body irradiation model. *Health Phys* 2014;**106**(6):772–86.
20. Blakely W, Sandgren D, Nagy V, Kim S-Y, Sigal G, Ossetrova N. Further biodosimetry investigations using murine partial-body irradiation model. *Radiat Prot Dosim* 2014;**159**(1-4):46–51.
21. Qu Y, Zhang B, Liu S, Zhang A, Wu T, Zhao Y. 2-Gy whole-body irradiation significantly alters the balance of CD4+ CD25– T effector cells and CD4+ CD25+ Foxp3+ T regulatory cells in mice. *Cellular Molecular Immunol* 2010;**7**(6):419–27.
22. Kroemer G, Galluzzi L, Kepp O, Zitvogel L. Immunogenic cell death in cancer therapy. *Annu Rev Immunol* 2013;**31**:51–72.
23. Wennerberg E, Lhuillier C, Vanpouille-Box C, Pilonis KA, García-Martínez E, Rudqvist N-P, et al. Barriers to radiation-induced in situ tumor vaccination. *Front Immunol* 2017;**8**:229.
24. Mondini M, Levy A, Mezzani L, Milliat F, Deutsch E. Radiotherapy–immunotherapy combinations—perspectives and challenges. *Molecular Oncology* 2020;**14**(7):1529–37.
25. Verhaegen F, Dubois L, Gianolini S, Hill MA, Karger CP, Lauber K, et al. ESTRO ACROP: Technology for precision small animal radiotherapy research: Optimal use and challenges. *Radiother Oncol* 2018;**126**(3):471–8.
26. Telarovic I, Kraysenbuehl J, Grgic I, Tschanz F, Guckenberger M, Pruschy M, et al. Probing spatiotemporal fractionation on the preclinical level. *Phys Med Biol* 2020;**65**(22):22NT02.
27. Butterworth KT, Ghita M, McMahon SJ, McGarry CK, Griffin RJ, Hounsell AR, et al. Modelling responses to spatially fractionated radiation fields using preclinical image-guided radiotherapy. *Br J Radiol* 2017;**90**(1069):20160485.
28. Sievert W, Stangl S, Steiger K, Multhoff G. Improved overall survival of mice by reducing lung side effects after high-precision heart irradiation using a small animal radiation research platform. *Int J Radiat Oncol Biol Phys* 2018;**101**(3):671–9.
29. Ghita M, Dunne VL, McMahon SJ, Osman SO, Small DM, Weldon S, et al. Preclinical evaluation of dose-volume effects and lung toxicity occurring in and out-of-field. *Int J Radiat Oncol Biol Phys* 2019;**103**(5):1231–40.
30. van Hoof SJ, Granton PV, Verhaegen F. Development and validation of a treatment planning system for small animal radiotherapy: SmART-Plan. *Radiother Oncol* 2013;**109**(3):361–6.
31. Gao H, Korn JM, Ferretti S, Monahan JE, Wang Y, Singh M, et al. High-throughput screening using patient-derived tumor xenografts to predict clinical trial drug response. *Nat Med* 2015;**21**(11):1318–25.
32. Ivashkevich A, Redon CE, Nakamura AJ, Martin RF, Martin OA. Use of the γ -H2AX assay to monitor DNA damage and repair in translational cancer research. *Cancer Lett* 2012;**327**(1-2):123–33.
33. Dewan MZ, Galloway AE, Kawashima N, Dewyngaert JK, Babb JS, Formenti SC, et al. Fractionated but not single-dose radiotherapy induces an immune-mediated abscopal effect when combined with anti-CTLA-4 antibody. *Clin Cancer Res* 2009;**15**(17):5379–88.
34. Chen D, Verma V, Patel RR, Barsoumian HB, Cortez MA, Welsh JW. Absolute lymphocyte count predicts abscopal responses and outcomes in patients receiving combined immunotherapy and radiation therapy: analysis of 3 phase 1/2 trials. *Int J Radiat Oncol Biol Phys* 2020;**108**(1):196–203.
35. Lambin P, Lieverse RI, Eckert F, Marcus D, Oberije C, van der Wiel AM, et al. Lymphocyte-sparing radiotherapy: the rationale for protecting lymphocyte-rich organs when combining radiotherapy with immunotherapy. *Semin Radiat Oncol* 2020 Elsevier.
36. Ganusov VV, Tomura M. Experimental and mathematical approaches to quantify recirculation kinetics of lymphocytes. Mathematical. In: *Computational and Experimental T Cell Immunology*. Springer; 2021. p. 151–69.
37. Ellsworth S, Balmanoukian A, Kos F, Nirschl CJ, Nirschl TR, Grossman SA, et al. Sustained CD4+ T cell-driven lymphopenia without a compensatory IL-7/IL-15 response among high-grade glioma patients treated with radiation and temozolomide. *Oncoimmunology* 2014;**3**(1):e27357.
38. Cao M, Cabrera R, Xu Y, Liu C, Nelson D. Different radiosensitivity of CD4+ CD25+ regulatory T cells and effector T cells to low dose gamma irradiation in vitro. *Int J Radiat Biol* 2011;**87**(1):71–80.
39. Beauford SS, Kumari A, Garnett-Benson C. Ionizing radiation modulates the phenotype and function of human CD4+ induced regulatory T cells. *BMC immunology* 2020;**21**(1):1–13.
40. Heylmann D, Ponath V, Kindler T, Kaina B. Comparison of DNA repair and radiosensitivity of different blood cell populations. *Sci Rep* 2021;**11**(1):2478.
41. Heylmann D, Rödel F, Kindler T, Kaina B. Radiation sensitivity of human and murine peripheral blood lymphocytes, stem and progenitor cells. *Biochimica et Biophysica Acta (BBA)-Reviews on Cancer* 2014;**1846**(1):121–9.
42. Cheng J-N, Luo W, Sun C, Jin Z, Zeng X, Alexander PB, et al. Radiation-induced eosinophils improve cytotoxic T lymphocyte recruitment and response to immunotherapy. *Sci Adv* 2021;**7**(5):eabc7609.
43. Buchwald ZS, Nasti TH, Lee J, Eberhardt CS, Wieland A, Im SJ, et al. Tumor-draining lymph node is important for a robust abscopal effect stimulated by radiotherapy. *J Immunother Cancer* 2020;**8**(2).
44. Marciscano AE, Ghasemzadeh A, Nirschl TR, Theodoros D, Kochel CM, Francica BJ, et al. Elective nodal irradiation attenuates the combinatorial efficacy of stereotactic radiation therapy and immunotherapy. *Clin Cancer Res* 2018;**24**(20):5058–71.
45. O'Melia MJ, Manspeaker MP, Thomas SN. Tumor-draining lymph nodes are survival niches that support T cell priming against lymphatic transported tumor antigen and effects of immune checkpoint blockade in TNBC. *Cancer Immunol, Immunotherapy* 2021:1–17.
46. Byun HK, Kim K-J, Han SC, Seong J. Effect of interleukin-7 on radiation-induced lymphopenia and its antitumor effects in a mouse model. *Int J Radiat Oncol* Biol* Phys* 2021;**109**(5):1559–69.
47. Du X, Tang F, Liu M, Su J, Zhang Y, Wu W, et al. A reappraisal of CTLA-4 checkpoint blockade in cancer immunotherapy. *Cell Res* 2018;**28**(4):416–32.
48. Sharma A, Subudhi SK, Blando J, Scutti J, Vence L, Wargo J, et al. Anti-CTLA-4 immunotherapy does not deplete FOXP3+ regulatory T cells (Tregs) in human cancers. *Clin Cancer Res* 2019;**25**(4):1233–8.
49. Quezada SA, Peggs KS. Lost in translation: deciphering the mechanism of action of anti-human CTLA-4. *Clin Cancer Res* 2019;**25**(4):1130–2.